Title
A Model for Aperiodicity in Earthquakes

Authors
Erickson, Brittany
Birnir, Bjorn
Lavallée, Daniel

Publication Date
2007-08-18

A Model for Aperiodicity in Earthquakes

Björn Birnir* Brittany Erickson† Daniel Lavallée‡

August 18, 2007

Abstract

Conditions under which a single oscillator model coupled with Dieterich-Ruina's rate and state dependent friction exhibits chaotic dynamics is studied. Properties of spring-block models are discussed. The parameter values of the system are explored and the corresponding numerical solutions presented. Bifurcation analysis is performed to determine the bifurcations and stability of stationary solutions and we find that the system undergoes a Hopf bifurcation to a periodic orbit. This periodic orbit then undergoes a period doubling cascade into a strange attractor, recognized as broadband noise in the power spectrum. The implications for earthquakes are discussed.

*Department of Mathematics, University of California, Santa Barbara, CA 93106-5080 (birnir@math.ucsb.edu).

†Department of Mathematics, University of California, Santa Barbara, CA 93106-5080 (brittany@math.ucsb.edu).

‡Institute of Crustal Studies, University of California, Santa Barbara, CA 93106-5080 (daniel@crustal.ucsb.edu).

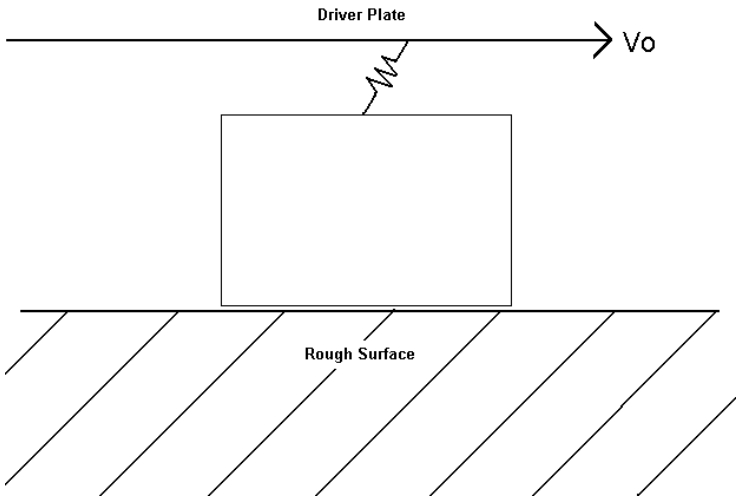

Figure 1: The single degree of freedom block and spring model is a slider coupled by a spring to a loader plate representing the other side of the fault. The surface upon which the block slips is rough and the friction force holding the slider in place is quite complex. Dieterich - Ruina style laboratory derived friction laws are used in this simulation for their capability in reproducing many qualitative dynamics similar to earthquake faulting.

1 Introduction

In the late 1960s, Burridge and Knopoff (BK) introduced a model that exhibited some characteristics similar to the dynamics of an earthquake fault [5]. They were interested in the role that friction plays in regard to the earthquake mechanism and how successive events relate to each other in time and space. The basic configuration of the BK model would consist of a block coupled by a spring to a moving loader plate representing the other side of the fault (see Figure 1). The equations of motion for this model include a friction term accounting for the roughness of the surface upon which the block slips. This term is a linear function of the velocity of the loader plate added to a viscous term proportional to the velocity of the block. Burridge and Knopoff wanted to see how many features observed in nature would be reproduced by their model.

Numerous studies and various improvements in this model have been attempted [16], [11], [7] in order to gain more realistic dynamics for simulations done to compare with laboratory experiments. Over the years it has been agreed upon that

friction constitutive laws are one of the most important factors in improving the laboratory model, enabling them to exhibit effects more like those observed in an actual fault. Additional references and discussion of this can be found in the paper [15] by Marone.

In the early 80s, rate and state dependent frictions laws have shown to be qualified in reproducing some behavior similar to that of earthquake faulting. Burridge and Knopoff incorporated a friction term in their model that was dependent on the block's velocity, but studies were later made that indicated that the friction term could not be a single valued function of velocity [15]. Improvements to the BK friction law were made by Dieterich, Ruina, Rice and others based on empirical studies of rock friction in the laboratory. They discovered that the incorporation of a state variable enabled the model to exhibit almost entirely the observed seismic behaviors such as stick-slip phenomena, fault healing and memory effects [20], [15]. Carlson and Batista developed further constitutive relations to describe the friction in a lubricated interface, with the state variable representing the degree of melting in the lubricant layer [6].

Dieterich-Ruina style friction in the spring-block model involves a logarithmic term whose nonlinearity has introduced additional difficulty in solving the problem. Due to the nonlinear term, analytic integration cannot be done even in the simplest case when one block is used. And while numerical solutions can be computed, the logarithmic term still proves to be a challenge. Under laboratory determined values for the parameters, the system is extremely stiff in the numerical sense. Due to the nonlinear term, the main source of numerical stiffness, extremely small times steps must be taken even with implicit methods. In the past, the Dieterich-Ruina friction term has been altered because of this problem. In [13] and [22], the authors regularize the nonlinear friction term for values near zero. This can be done by either allowing rate values to be of either sign and taking absolute values or by linearizing the term giving only a close approximation in a small interval. This alteration of the nonlinear term may explain why chaotic regimes have rarely been observed.

In this paper we use the full nonlinear term in the numerics and find many different types of solutions to the system of a single block. Figure 2 shows the dynamics of the single block from Figure 1, under such a new friction law, exhibiting periodic behavior. As shown later, this periodic orbit undergoes a period-doubling cascade into a strange attractor due to variations in the system's parameters. [21] used unimodal maps to show that chaotic behavior was suggested by this friction force. In 1999, [10] found dynamic regimes similar to ours while experimenting with lubricant films subjected to shear. The measured friction force remained constant for the steady sliding phase, oscillatory between two values for periodic phases, and even chaotic in a certain velocity range. These empirical results suggest that the nonlinearity of the

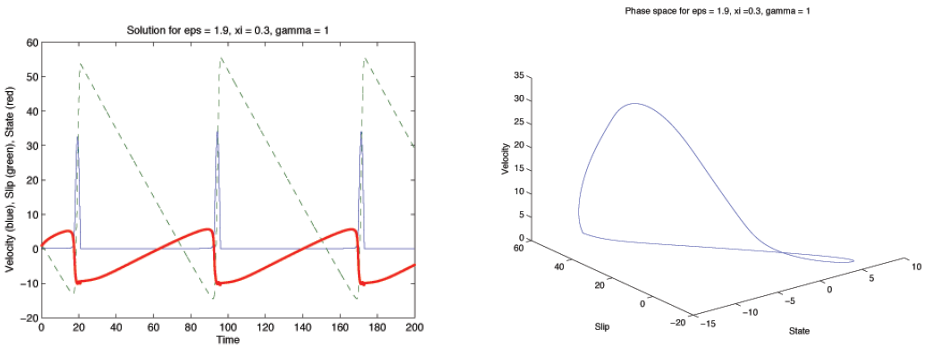

Figure 2: Solution to Single-Degree of Freedom system (2) with parameters $\epsilon = 1.9$, $\xi = 0.3$, $\gamma = 1$. Left: The slip value (green), characterizes the block sticking and slipping. The velocity (blue) is initially at zero, while the block is stuck. The slider remains stuck until the friction force holding it in place is overcome by the loading force. The velocity then spikes when the block slips and the slip value jumps almost instantaneously. The velocity then returns to zero, as the block becomes stuck and another cycle begins. The state variable (red) measures the amount of asperity contact that the block has with the surface. While the block is stuck, the contacts steadily increase, until the block slips and the contacts instantly decrease. Right: periodic orbit in the corresponding phase space.

friction force in these models is crucial for chaotic dynamics to emerge.

We integrate the dynamical system numerically, choosing parameter values that are commonly used in more recent literature. Under the assumption that the friction law is the main physical process regulating the frequency of earthquakes, then the presence of a strange attractor suggests first that earthquakes are sensitive to perturbations. Second, the strange attractor suggests that earthquakes are typically aperiodic, although periodic earthquakes have been observed [2], [23]. Thus aperiodic orbits on the strange attractor may exhibit dynamics analogous to those during an earthquake.

2 The Single Degree of Freedom Model

We began numerical simulations of a spring-block model by using Madariaga's [14] version of a single degree of freedom oscillator. In this form one can view the slider's slip relative to the pulling force or driver plate. These equations of motion coupled with Dietrich and Ruina's (DR) rate and state dependent friction law [20], [19], are given by:

$$\left.\begin{aligned} \dot{\theta} &= -(v/L)(\theta + Blog(v/v_0)) \\ \dot{u} &= v - v_0 \\ \dot{v} &= (-1/M)[ku + \theta + Alog(v/v_0))] \end{aligned}\right\}, \tag{1}$$

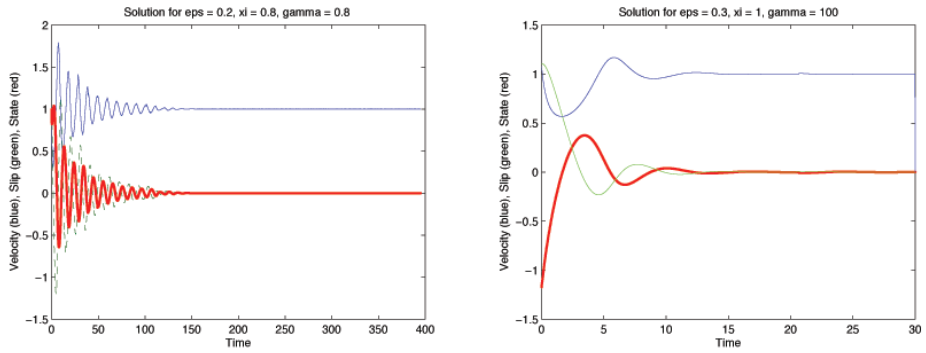

Figure 3: Stationary solutions of system (2) whose parameter values have not crossed the Hopf bifurcation plane in Figure 6. $(\epsilon, \xi, \gamma) = (0.2, 0.8, 0.8)$ and $(\epsilon, \xi, \gamma) = (0.3, 1, 100)$ yield stationary solutions corresponding to no movement of the block relative to the driver plate. After a transient region, its velocity stays at a constant rate $v = 1$ as it moves with the driver plate. Its relative slip is zero and its change in state (asperity contacts) is also zero.

which can be non-dimensionalized by defining the new variables $\hat{\theta}$, $\hat{v}$, $\hat{u}$ and $\hat{t}$ in the following way. Set $\theta = A\hat{\theta}$, $v = v_o\hat{v}$, $u = L\hat{u}$, $t = (L/v_o)\hat{t}$ then returning to the use of θ, v, u and t. This non-dimensionalization puts the system into the following form:

$$\left.\begin{aligned} \dot{\theta} &= -v(\theta + (1+\epsilon)log(v)) \\ \dot{u} &= v - 1 \\ \dot{v} &= -\gamma^2[u + (1/\xi)(\theta + log(v))] \end{aligned}\right\}, \tag{2}$$

where θ is the state variable, u is the slip, v is the loading velocity, v_o is a reference velocity, $\epsilon = (B-A)/A$ measures the sensitivity of the velocity relaxation, $\xi = (kL)/A$ is the nondimensional spring constant, and $\gamma = \sqrt{k/M}(L/v_o)$ is the nondimensional frequency. It is important to note that the parameter values currently being used in the literature are approximately $\epsilon = 3.1$, $\xi = 0.5$ and $\gamma = 10^4 - 10^{12}$ [14].

The system has only one stationary solution, namely $(\theta, u, v) = (0, 0, 1)$, which corresponds to steady sliding. This solution is plotted in Figure 3 under two different sets of parameter values. In this case, the numerical solution falls into its stationary state after a transient region and corresponds to no movement of the block relative to the driver plate. The block's velocity is the same as that of the driver plate, thus its slip remains zero. Investigation of the local eigenvalues of system (2) will inform us as to what parameter combinations lead to bifurcations of the stationary solution, as well as how to choose a suitable numerical scheme. The Jacobian matrix Df is evaluated at the stationary solution to obtain matrix A:

$$A = \begin{bmatrix} -1 & 0 & -(1+\epsilon) \\ 0 & 0 & 1 \\ -\gamma^2/\xi & -\gamma^2 & -\gamma^2/\xi \end{bmatrix}$$

The corresponding eigenvalues of A are computed and we find that the system has one non-zero real eigenvalue and a pair of complex conjugates, suggesting the possibility of a Hopf bifurcation to occur. When the matrix A has a simple pair of pure imaginary eigenvalues and no other eigenvalues with zero real part, then if the complex eigenvalues cross the imaginary axis, the stationary solution will Hopf bifurcate into a periodic orbit. See [12] and [17] for more information about this bifurcation.

3 Numerical Integration and Analysis

In computing the local eigenvalues of Df at different times along a solution's trajectory, we found that when the block's velocity $v \to 0$, the minimum eigenvalue of Df is $<< 1$ and decays exponentially towards $-\infty$ as the parameter γ is increased. This is important to consider because for commonly used values of γ ($\gamma \approx 10^4 - 10^{12}$ according to [14]) the more negative the eigenvalue is, the stiffer the system will be. In regular systems, the choice of the time step should be chosen to satisfy accuracy requirements, and methods such as forward Euler and explicit Runge-Kutta methods can be used. In stiff systems, however, these explicit methods are numerically unstable and require very small time steps in order to maintain numerical stability. Implicit methods have the ability to remain stable even with larger time steps, thus we chose to use an implicit, second order backward-differentiation formula (BDF) numerical scheme from [1]. See appendix A for a summary of this method applied to system (2).

While the BDF scheme is stable, we find that the nonlinearity of the logarithm term restricts our time step nonetheless. System (2) is stiff in time intervals where v approaches zero, i.e. if the step size is too large, then v can be computed to be negative (or zero). Evaluating $log(v)$ at this time returns either an imaginary or undefined number and thus a completely inaccurate solution. If the step size is taken small enough, the velocity will move away from zero, due to the negative coefficient $-\gamma^2/\xi$. Thus higher values of γ will increase the stiffness in the system and require an extremely small time step. It appears that the time step Δt scales inversely with γ ($\Delta t \approx k\gamma^{-1}$ for some constant k), but no in-depth studies have been done on this.

We have found that for small values of ϵ, stationary, period one and period two orbits result. In integrating this system numerically, solutions that were stationary Hopf bifurcate and periodic orbits are born. It is possible to calculate the parameter

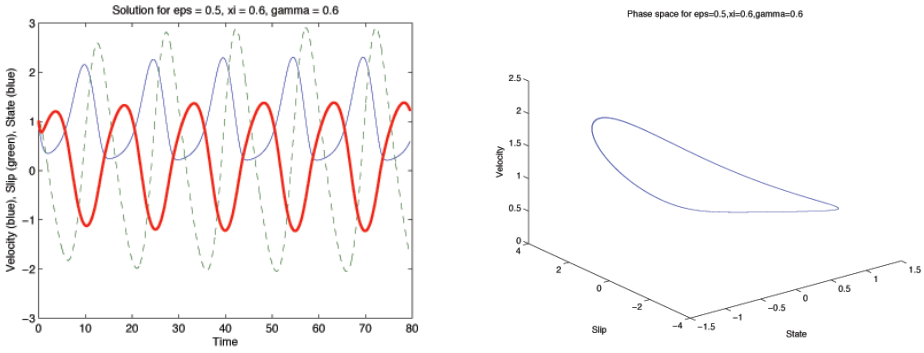

Figure 4: Periodic solution of system (2) whose parameter values have crossed the Hopf bifurcation plane (given by Figure 6) and its associated phase space. $(\epsilon, \xi, \gamma) = (0.5, 0.6, 0.6)$ yields a period one orbit relatively smooth in its dynamics. The slip (green) fluctuates, increasing as the velocity (blue) peaks and decreasing as the velocity approaches zero. Similarly the state variable (red) decreases when the velocity peaks, but grows when the velocity reaches a minimum, and the asperity contacts are reestablished. The corresponding phase portrait on the bottom is a smooth circular orbit where the periodicity between the velocity, slip and state is further clarified.

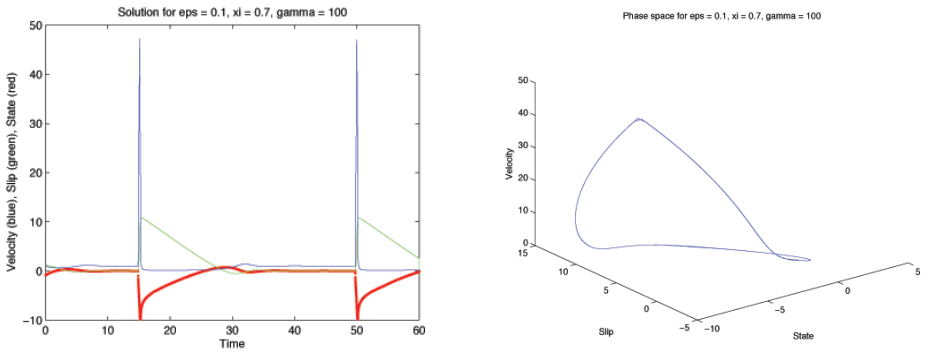

Figure 5: Periodic solution of system (2) whose parameter values have crossed the Hopf bifurcation plane (given by Fig. 6) and its associated phase space. $(\epsilon, \xi, \gamma) = (0.1, 0.7, 100)$ yields a period one orbit with similar dynamics to those in Figure 4, but the changes in the velocity, slip and state are more sharp and distinguishable, corresponding to a more abrupt movement of the block relative to the driver plate. The associated phase portrait is also a circular orbit but not quite as smooth as that in Figure 4.

regions for which this bifurcation occurs as we have done in Figure 6. Interestingly, for higher values of γ the surface is two dimensional, suggesting that the bifurcation plane is actually independent of γ. Figures 4 and 5 represent two period one orbits similar to the one in Figure 2. The solution in Figure 4 is a periodic solution but is more smooth in its motion than that in Figure 5 (or in Figure 2) that represent more abrupt motion of the block slipping beyond the driver plate. Initially the block is stuck on a rough surface so the relative slip to the driver plate decreases at a constant rate as the driver plate catches up and even surpasses the block. Once the pulling force overcomes the static friction holding the block in place, the block's velocity spikes, the slider shoots forward again and another cycle begins. The smoothness in the dynamics of Figure 4 represents a fluid-like interaction between the block and the rough surface it slides upon. The block fluctuates gently in response to the driver plate and the friction on the surface, but never completely sticks to it for any period of time. Note that when the velocity increases, the state variable decreases, a fact that supports the interpretation that the state variable measures the amount of contact the block has with the surface: when the block is stuck, the contacts will be greater than when the block is in motion. After the block arrests and comes to a stop, the contacts begin to increase, a process that could be interpreted as fault healing after an event.

Periodic solutions can be viewed in the phase space, or by plotting the corresponding Poincaré map as shown in the right of Figure 7. The map is constructed by slicing a transverse hyperplane through the periodic solution in the phase space and taking a small neighborhood around the solution in the hyperplane [12]. Stationary solutions will, in general, not appear on the Poincaré map. Period one orbits correspond to a fixed point of the Poincaré map, period two orbits will appear as two points on the Poincaré map etc., and chaotic orbits are represented by randomly distributed points on the map.

After a sequence of period doubling bifurcations, chaotic orbits appear in the phase space, seen in the left of Figure 7. These chaotic orbits are all pulled into what's known as an *attractor* in the phase space. An attractor is a compact set in the phase space, invariant under the flow and with a shrinking neighborhood to which orbits of the system are attracted. It is called a *strange attractor* if it exhibits sensitive dependence on initial conditions. See [12] and [17] for more details on this topic. If we consider the bifurcation diagram of the solution $X(t) = (\theta(t), u(t), v(t))$ as a function of ϵ (viewed in the right of Figure 7), then there is an initial interval where the attractor is a stationary solution. Then a Hopf bifurcation occurs and the attractor is a fixed point of the Poincaré map corresponding to a periodic orbit of system (2). As seen in the right of Figure 7, the system undergoes a Hopf bifurcation around $\epsilon \approx 4$. Then a series of period doubling bifurcations occur and we get a sequence of intervals where the attractors are stable periodic orbits of period 4, 8,

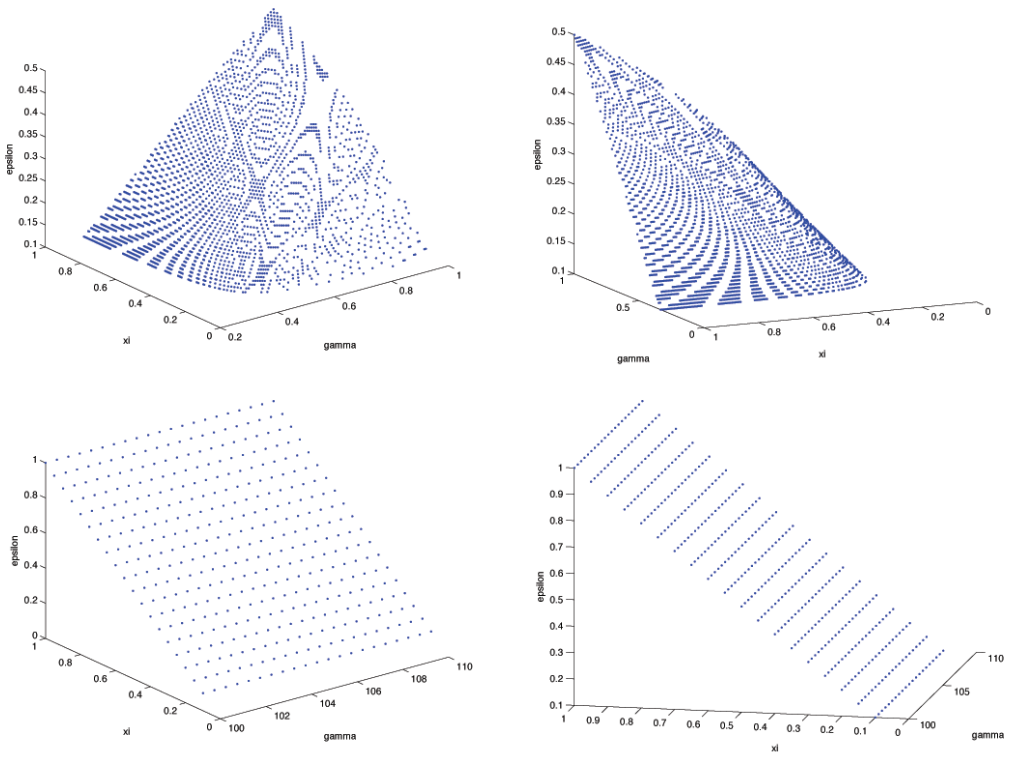

Figure 6: Two Hopf Bifurcation Planes: Parameter spaces (from two different angles) for system (2) that yield a Hopf bifurcation. Parameter combinations that lie below these surfaces will yield stationary solutions, while combinations above it will yield periodic solutions. Top: Small values of γ produce a surface in the ϵ, ξ, γ plane as do larger values of γ (bottom), although this surface appears to be independent of γ.

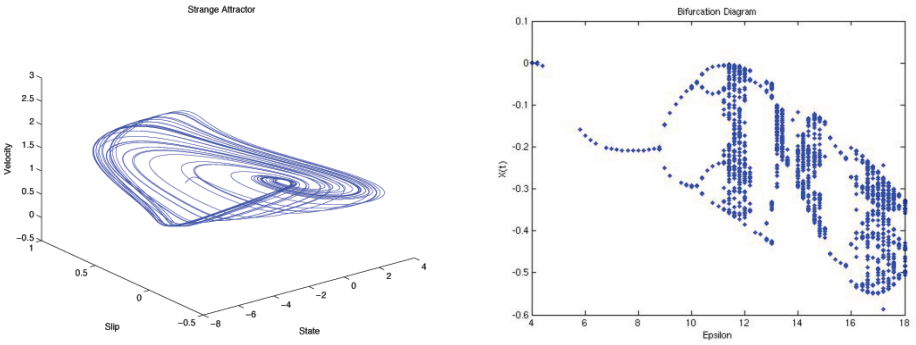

Figure 7: Left: The strange attractor appears in the phase space of a single block after ϵ passes through a critical value. The attractor is a compact set, invariant under the flow and with a shrinking neighborhood to which orbits of the system approach. In our case, the attractor is an aperiodic orbit and that it is strange is determined by the system's sensitive dependence on initial conditions, yielding broadband noise in the power spectrum. Right: Critical values of ϵ yield period doubling bifurcations of periodic orbits. The Poincaré map is shown on the vertical axis, and the parameter ϵ on the horizontal axis.

16 etc. This period doubling cascade converges around $\epsilon = 11.5$, where a strange attractor appears [8]. If we assume that the nonlinear friction term in a single block system is responsible for simulating aperiodicity in earthquakes then it requires that ϵ be at least in this regime.

These period-doubling bifurcation points, ϵ_n, converge at ϵ_∞, where $\lim_{n\to\infty} \epsilon_n = \epsilon_\infty \approx 11.5$, and the attractor becomes a *singularly supported strange attractor* with a histogram given in the top of Figure 8. This means that the attractor consists of a thin (measure zero) set on the x-axis. Notice that in each interval the periodic orbit from the previous interval survives but becomes unstable. Thus each interval to the left of ϵ_∞ contains unstable periodic orbits of all the previous periods.

What can we say about the region beyond ϵ_∞? It is known that the set of ϵ for which there exists no stable periodic orbit has positive Lebesgue measure and the slightly smaller set for which there is sensitive dependence on initial conditions also has positive Lebesgue measure. It has been proven more recently that the still smaller set where there exists *absolutely continuous invariant measures* living on support of the attractor on the x-axis has positive Lebesgue measure, as seen in the bottom of Figure 8 [3]. For these values of ϵ the dynamics reduce to ergodic theory on the strange attractor using the absolutely continuous invariant measure. In particular the ergodic theorem holds so we can exchange time averages by space averages (on the attractor) and the motion is mixing [3], [8]. For values of ϵ past 12, there are windows (open sets in ϵ) where the attractor returns to a periodic orbit from a chaotic one.

To confirm our results we calculated the Fourier power spectrum for period 1, 2 and chaotic orbits, shown in Figure 9. We took the numerical solution to the

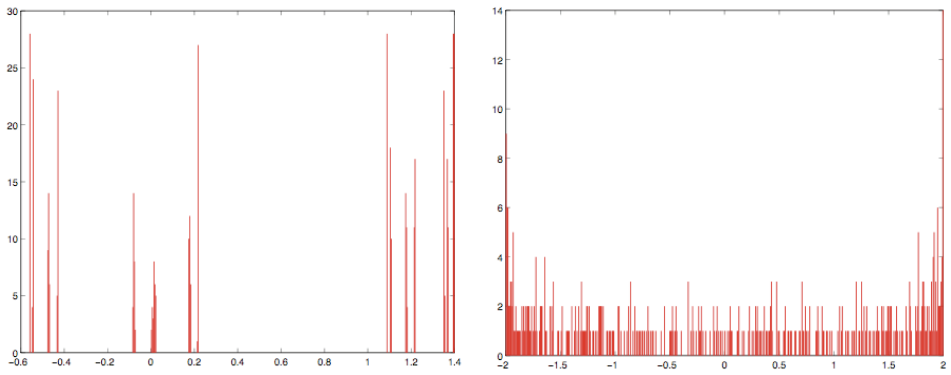

Figure 8: Histograms for a singularly supported attractor (left) and an attractor with an absolutely continuous invariant measure (right). These figures are for the quadratic map. The x-axis is the interval where the map takes its values and the y-axis is the number of points that hit each x value (5000 points are sampled).

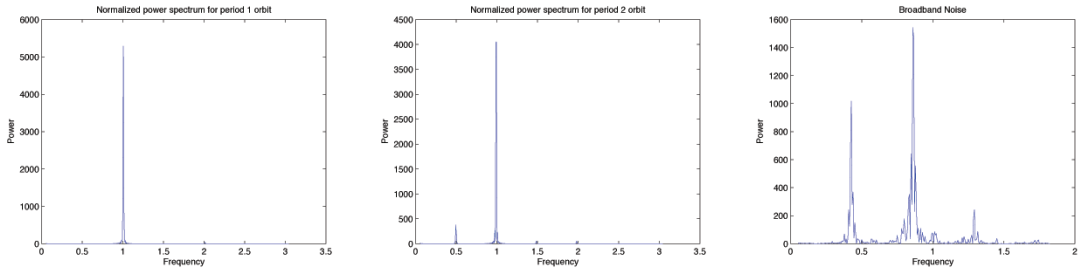

Figure 9: The Fourier power spectrum was taken for period 1,2 and chaotic orbits. It plots the mean squared amplitude of the Fourier transform of the slip, $\hat{u}(f_k)$, against the positive frequencies f_k for $k = 0, ..., N-1$. The bifurcation from period 1 to 2 is confirmed in the first two figures, and the broadband noise in the far right Figure indicates that the attractor is strange.

block's slip, $u(t_n)$ at N discrete points, and computed its discrete Fourier transform, $\hat{u}(f_k)$ for $k = 0, ..., N-1$. The estimated power $P(f_k) := |\hat{u}(f_k)\bar{\hat{u}}(f_k)|/N^2$ where $f_k := k/\Delta t$ and $\bar{u}$ is the conjugate of u [18]. The power spectrum will plot the mean squared amplitude of $\hat{u}(f_k)$ against the positive frequencies f_k for $k = 0, ..., N-1$. After normalizing the frequencies, the bifurcation from period one to period two is confirmed in the first two plots in Figure 9. In the first plot, the single peak in power at frequency = 1 corresponds in period to one dominate Fourier coefficient in the Fourier expansion of the numerical solution. After the bifurcation, a first peak appears at frequency = $\frac{1}{2}$, i.e, double the period of the previous solution, and a second peak appears at frequency = 1, indicating a period two orbit. The broadband noise in the third plot in Figure 9 indicates that the attractor is indeed strange [4], [9].

4 The Three Degree of Freedom Model

It is interesting to note that under Dieterich-Ruina style friction, chaotic dynamics resulted even with the use of one block. The chaotic region however, required that ϵ be larger than commonly used values of the parameter. A larger system is explored to see where the threshold for chaos lies, and we find that chaotic dynamics emerge for smaller parameter values than those used in the single block system. We built the three block system under Newton's second law and the equations of motion found in BK's original paper.

We let x_j represent the displacement from equilibrium of the jth block. Thus with μ_{j+1} as the spring constant connecting the jth block to the $j+1th$ block, and λ_j as the spring constant connecting the jth block to the driver plate, which is moving at a constant rate v_o, our equations become:

$$m_j\ddot{x_j} = \mu_{j+1}(x_{j+1} - x_j) - \mu_j(x_j - x_{j+1}) - \lambda_j(x_j - v_o t) + F_j,$$

for j = 1, 2 and 3. We have identified the first and last block with each other to make the system periodic and taken spring constants to be equal. We want to view the slip of the jth block with respect to the driver plate, so we introduce the new variable: $u_j = x_j - v_0 t$. Thus $\dot{u_j} = v_j - v_0$ where $v_j = \dot{x_j}$. Re-writing as a non-dimensionalized set of first order equations and applying DR's friction law (for F_j) yields:

$$\left.\begin{aligned} \dot{\theta_j} &= -v_j(\theta_j + (1+\epsilon)log(v_j)) \\ \dot{u_j} &= v_j - 1 \\ \dot{v_j} &= \gamma^2[u_{j-1} - 2u_j + u_{j+1} - u_j - (1/\xi)(\theta_j + log(v_j))] \end{aligned}\right\} \tag{3}$$

where the parameters, ϵ, ξ, γ remain those in section 2, and all variables are non-dimensionalized versions of those in equations (2). We proceed by the computations

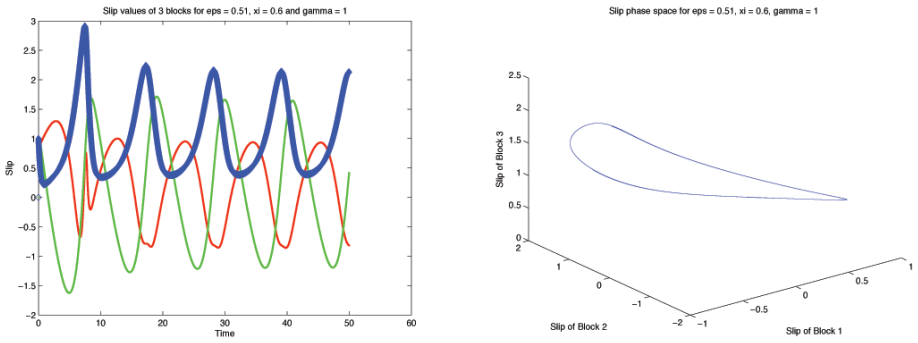

Figure 10: Slip values of three different blocks for period two orbit with $\epsilon = 0.51, \xi = 0.6, \gamma = 1$

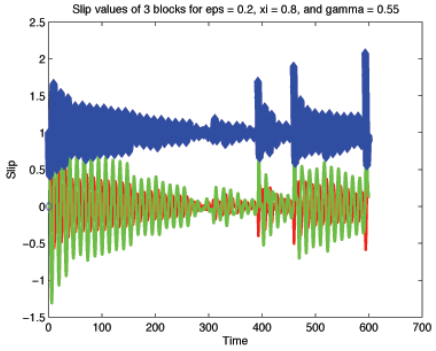

Figure 11: Slip values of the three different blocks for an aperiodic solution with $\epsilon = 0.2, \xi = 0.8, \gamma = 0.55$

preformed to the system in section 2, first computing the Jacobian matrix for system (3) evaluated at its stationary solution and finding its associated eigenvalues.

We notice that if we increase the same parameter ϵ, and strongly couple the blocks so that they are not allowed to move very independently, (i.e. we set $\xi = 0.6$), then the system undergoes a similar bifurcation from a stationary solution to a periodic orbit as the one block system. Some further exploration into parameter combinations leads to a period two orbit. The important difference from the single degree of freedom model (2) is that these period doublings occur for a range of parameter values comparable to those derived in the laboratory. Figure 10 shows a plot for parameters on the order of 10^{-1}, i.e., a much smaller value than for the single block. When ϵ is further increased we find aperiodic orbits like that in Figure 11 and conclude that for the system of three blocks, the threshold for chaos is greatly lowered for values of ξ and ϵ. The route to chaos for very large values of γ remains an open question.

5 Conclusions

We have shown that the single degree of freedom block and spring model (2) with the Dieterich-Ruina friction law exhibits complex behavior. This result suggests that the friction law can be a potential source for the observation of aperiodicity in earthquake dynamics. By using the full nonlinearity of the friction term, we see that for a set of parameter values, the system remains in a stationary state. An increase in the parameter ϵ forces the system to undergo a Hopf bifurcation from a stationary solution to a periodic orbit, some of which exhibit stick slip behavior reminiscent of earthquake dynamics. The periodic orbit then undergoes a period doubling bifurcation initiating a period doubling cascade where we find periodic orbits of period 2, 4, 8, 16 etc. When ϵ reaches ϵ_∞, the periodic orbit bifurcates into an aperiodic orbit on a singularly supported strange attractor. Past ϵ_∞, there exists absolutely continuous invariant measures living on support of the attractor and we find windows in which periodic orbits appear and then bifurcate into aperiodic orbits.

These different solutions, from periodic to chaotic, can be associated to periodic and aperiodic earthquake dynamics. It is important to note that non-periodic behavior observed in this simple problem may be partially responsible for irregular ground motion in addition to the heterogeneity in the stress distribution as simulated in [13]. Furthermore, it will be important to see how this non-periodic behavior will affect the nucleation process in the numerical simulation of sequences of earthquakes. Our results suggest that the use of the nonlinear friction term generates chaotic regimes that approximations to the term may not produce. There are also empirical results from the laboratory, obtained by [10], whose friction measurements suggest the presence of a strange attractor. Because it is possible to calculate the stiffness of system (2) at different times, a stiff solver seems to be the method of choice given high values of γ for which an extremely small time step is required. Rather than regularize the nonlinear friction term as done previously in [13] and [22], it is possible to numerically integrate the system without an approximation to the friction term. Although we cannot yet study the bifurcations of solutions for higher values of γ, it is possible to calculate parameter spaces for which Hopf bifurcations occur and determine the chaotic regimes for this system.

6 Acknowledgements

The authors were supported by grants number DMS-0352563 from the National Science Foundation whose support is gratefully acknowledged. We would like to thank Alethea Barbaro and Eric Daub at UCSB for their insight and helpful suggestions. We would also like to thank George O. Mohler at UCSB for his advice on numerical methods used for this paper.

A Backward Differentiation Formula (BDF):

The BDF method solves the differential equation: $\mathbf{y}' = \mathbf{f}(t, \mathbf{y})$. It is derived by taking a second order approximation to $\mathbf{y}'$ by:

$$\mathbf{y}' \approx \frac{3\mathbf{y}_n - 4\mathbf{y}_{n-1} + \mathbf{y}_{n-2}}{2h}$$

Given the initial condition, $\mathbf{y}_1$, one step of backward Euler is done to obtain $\mathbf{y}_2$ and the BDF scheme is ready to be implemented:

$$3\mathbf{y}_n - 4\mathbf{y}_{n-1} + \mathbf{y}_{n-2} = 2h\mathbf{f}(t_n, \mathbf{y}_n)$$

Since $\mathbf{f}(\mathbf{t}, \mathbf{y})$ is usually a nonlinear function, we rewrite the scheme as:

$$3\mathbf{y}_n - 4\mathbf{y}_{n-1} + \mathbf{y}_{n-2} - 2h\mathbf{f}(t_n, \mathbf{y}_n) = 0$$

and at every time step, apply Newton's method to solve the root problem.

For every fixed step in time, n, the $\mathbf{y}_n^{\nu+1th}$ iteration under Newton's method is given by:

$$\mathbf{y}_n^{\nu+1} = \mathbf{y}_n^{\nu} - (3I - 2hD\mathbf{f}(t_n, \mathbf{y}_n^{\nu}))^{-1}(3\mathbf{y}_n^{\nu} - 4\mathbf{y}_{n-1} + \mathbf{y}_{n-2} - 2h\mathbf{f}(t_n, \mathbf{y}_n^{\nu})),$$

where the vectors $\mathbf{y}_n^\nu$ and $\mathbf{f}(t_n, \mathbf{y}_n^\nu)$ are given by,

$$\mathbf{y}_n^\nu = \begin{bmatrix} \theta_n^\nu \\ u_n^\nu \\ v_n^\nu \end{bmatrix}$$

$$\mathbf{f}(t_n, \mathbf{y}_n^\nu) = \begin{bmatrix} -v_n^\nu(\theta_n^\nu + (1+\epsilon)log(v_n^\nu)) \\ v_n^\nu - 1 \\ -\gamma^2(u_n^\nu + (1/\xi)(\theta_n^\nu + log(v_n^\nu)) \end{bmatrix}$$

and the matrix $D\mathbf{f}(t_n, \mathbf{y}_n^\nu)$ is

$$D\mathbf{f} = \begin{bmatrix} -v_n^\nu & 0 & -\theta_n^\nu - (1+\epsilon)(log(v_n^\nu)+1) \\ 0 & 0 & 1 \\ -\gamma^2/\xi & -\gamma^2 & (-\gamma^2/\xi)(1/v_n^\nu) \end{bmatrix}$$

References

[1] Ascher, U. M. and Petzold, L. R.: Computer methods for ordinary differential equations and differential-algebraic equations, SIAM, Philadelphia, 1st edition, 1998.

[2] Beeler, N. M., Lockner, D. L., and Hickman, S. H.: A simple stick-slip and creep-slip model for repeating earthquakes and its implication for microearthquakes at parkfield, Bull. Seism. Soc. Am., 91, 1797–1804, 2001.

[3] Benedicks, M., and Young, L.: Absolutely continuous invariant measures and random perturbations for certain one-dimensional maps, Ergod. Th. and Dynam. Sys., 12, 13–37, 1992.

[4] Bergé, P., Pomeau, Y., and Vidal, C.: Order within chaos: towards a deterministic approach to turbulence. Herman, Paris, 1st edition, 1984.

[5] Burridge, R., and Knopoff, L: Model and theoretical seismicity, Bull. Seism. Soc. Am., 57, 341–371, 1967.

[6] Carlson, J. M. and Batista, A. A.: Constitutive relation for the friction between lubricated surfaces, The American Physical Society, 53, 4153–4165, 1996.

[7] Clancy, I. and Corcoran, D: Criticality in the burridge-knopoff model, Phys. Rev. R, 71, 335–339, 2005.

[8] Collet, P. and Eckmann, J. P.: Iterated maps on the interval as dynamical systems, Birkhauser, Philadelphia, 1st edition, 1980.

[9] Crutchfield, J., Farmer, D., Packard, N., Shaw, R., Jones, G., and Donelly, R.J.: Power spectral analysis of a dynamical system, Physics Letters A, 76,1–4, 1980.

[10] Drummond, C.: Nanotribology of confined thin films, Ph.D, University of California at Santa Barbara, Santa Barbara, CA, 1999.

[11] Gross, S.: Traveling wave and rough fault earthquake models: illuminating the relationship between slip deficit and event frequency statistics, Am. Geophys. Union, 88, 10,359–10,370, 2000.

[12] Guckenheimer, J. and Holmes, P.: Nonlinear oscillations, dynamical systems, and bifurcations of vector fields, Springer-Verlag, New York, 1st edition, 1983.

[13] Lapusta, N. and Rice, J. R.: Nucleation and early seismic propagation of small and large events in a crustal earthquake model, J. Geophys. Res., 108, 1–18, 2003.

[14] Madariaga, R.: Study of an oscillator of single degree of freedom with dieterich-ruina rate and state friction, Laboratoire de Géologie, Ecole Normale Supérieure, Unpublished Notes (Preprint), 1998.

[15] Marone, C.: Laboratory-derived friction laws and their application to seismic faulting, Annu. Rev. Earth Planet. Sci., 26, 643–696, 1998.

[16] Pelletier, J. D.: Spring-block models of seismicity: review and analysis of a structurally heterogeneous model coupled to a viscous asthenosphere, Geophysical Monograph, 120, 27–42, 2000.

[17] Perko, L.: Differential equations and dynamical systems, Springer-Verlag, New York, 3rd edition, 2001.

[18] Press, W. H., Teukolsky, S. A., Vetterling, W. T., and Flannery, B. P.: Numerical recipes in fortran, Cambridge University Press, New York, 2nd edition, 1986.

[19] Rice, J. R. and Tse, S. T.: Dynamic motion of a single degree of freedom system following a rate and state dependent friction law, J. Geophys. Res., 91, 521–530, 1986.

[20] Ruina, A.: Slip instability and state variable friction laws, J. Geophys. Res., 88, 10359–10370, 1983.

[21] Shkoller, S. and Minster, J. B.: Reduction of dietrich-ruina attractors to unimodal maps, Nonlin. Processes Geophys., 4, 63–69, 1997.

[22] Szkutnik, J., Kawecka-Magiera, B., and Kulakowski, K.: History-dependent synchronization in the burridge-knopoff model, `http://www.citebase.org/abstract?id=oai:arXiv.org:nlin/0310030`, 2003.

[23] USGS: Earthquake hazards program northern california, `http://quake.usgs.gov/research/parkfield/repeat.html`, 2002.